Supporting Information

Dissecting the mechanism of the non-heme iron endoperoxidase FtmOx1 using substrate analogs

Guoliang Zhu[a‡], Wupeng Yan[b‡], Xinye Wang[a‡], Ronghai Cheng[c‡], Nathchar Naowarojna[c], Kun Wang[a], Jun Wang[b], Heng Song[d], Yuyang Wang[a], Hairong Liu[e], Xuekui Xia[e], Catherine E. Costello[c], Xueting Liu[a]*, Lixin Zhang[a]*, Pinghua Liu[c]*

[a]State Key Laboratory of Bioreactor Engineering, East China University of Science and Technology, Shanghai, 200237, China

[b]School of Life Sciences and Biotechnology, Shanghai Jiao Tong University; Shanghai, 200237, China.

[c]Department of Chemistry, Boston University, Boston, MA, 02215, USA.

[d]College of Chemistry and Molecular Sciences, Wuhan University, Wuhan, Hubei Province, 430072, China.

[e]Key Biosensor Laboratory of Shandong Province, Biology Institute, Qilu University of Technology (Shandong Academy of Sciences), Jinan, Shandong Province, 250013, China.

‡These authors contributed equally.

*Corresponding authors. Email: liuxt2010@126.com (X. Liu), lxzhang@ecust.edu.cn (L. Zhang), and pinghua@bu.edu (P. Liu)

Table of Contents

Experimental Procedures

General

NMR spectra were acquired on an Agilent DD2 600 MHz spectrometer (600 MHz for ^{1}H-NMR and 150 MHz for ^{13}C-NMR) (Santa Clara, CA, USA). NMR spectra were recorded in DMSO-d_6 (99.9 atom% enriched, AICON) and $CDCl_3$ (99.5 atom% enriched, Kanto). ^{1}H-NMR chemical shifts were reported in δ value based on residual DMSO-d_6 (2.50 ppm) and $CDCl_3$ (7.26 ppm) as reference. ^{13}C-NMR chemical shifts were reported in δ value based on DMSO-d_6 (39.52 ppm) and $CDCl_3$ (77.16 ppm) as a reference. Data are reported as follows: chemical shift, multiplicity (s = singlet, d = doublet, t = triplet, q = quartet, m = multiplet), coupling constant (Hz), and integration. LC-HR-MS(ESI) measurements were obtained on Thermo Q Exactive Orbitrap mass spectrometer coupling with a Shimadzu LC-20AD UPLC equipped with a Waters ACQUITY BEH C18 column (2.1 × 100 mm, 1.7 μm particles). The LC-MS analysis was run using an Agilent 1100 Series separation module with an Agilent G1956B MS detector. RP-HPLC was performed on an Agilent 1260 Series separation module with a diode array detector. HPLC analysis was carried out using a C18 column (ACE Excel 5 C18, 4.6 × 250 mm, 5 μm, 1 ml/min). Semipreparative HPLC was carried out using a C18 column (Titank, 10 × 250 mm, 5 μm, 4 ml/min). Protein-substrate complexes were first screened for crystallization using a Crystal Gryphon auto dispenser (Art Robbins Instruments, LLC), optimized crystals were sent to the Shanghai Synchrotron Radiation Facility (SSRF) to collect X-ray diffraction data under beamline BL02U1 and BL19U1 with a Pilatus3 6M image plate detector. Biological reagents, chemicals, and media were purchased from standard commercial sources unless stated otherwise.

Fermentation of *Aspergillus fumigatus* Af293 and purification of fumitremorgin B (1), verruculogen (2), and 12,13-dihydroxy-fumitremorgin C (4)

Strain *A. fumigatus* Af293 cells were cultured on PDA medium at 25°C for 3 days, and agar plugs (5-mm-diameter) were placed into 10 Erlenmeyer flasks (250 ml), each containing 100 ml of potato dextrose broth (PDB). The flasks were incubated at 28°C on a rotary shaker at 220 rpm for 3 days to generate the seed culture, from which 5 ml of culture was separately inoculated into 200 aseptic-bags, each containing 80 g of autoclaved rice and 120 ml distilled H_2O. These aseptic-bags were transferred to an incubator and fermented at 28°C for 30 days. Then, 16 kg of whole cultures were extracted with EtOAc (3 × 30 L) and concentrated under reduced pressure to yield a dark brown gum (61 g).

The crude extracts were fractionated by silica gel vacuum liquid chromatography (85 × 300 mm column packing with 300 g 300~400 mesh silica gel) using a CH_2Cl_2-MeOH gradient (100:0, 99:1, 98:2, 97:3, 96:4, and 0:100; each 2800 ml) to afford 6 fractions (G1–G6). Fraction G3 (10.5 g), dissolved in CH_2Cl_2 and MeOH (1:1), was applied to a Sephadex LH-20 column (45 × 1200 mm packing with 1600 ml resin) using MeOH as the mobile phase to yield 11 sub-fractions (G3N1–G3N11). LC-MS analysis of these fractions revealed the existence of the target compounds (fumitremorgin B and verruculogen) in fraction G3N3 based on characteristic UV absorption and

HR-ESI-MS spectra. Then, G3N3 (65.6 mg) was further purified by semi-preparative RP-HPLC using a C18 column (Titank, 10 × 250 mm, 5 μm) with a flow rate of 4.0 ml/min and a gradient elution (During 0–16 min, ACN was increased from 10% to 99% in 0.1% HCOOH-containing H_2O and then the column was eluted for 5 mins with 99% ACN in 0.1% HCOOH-containing H_2O) to obtain fumitremorgin B (**1**, 35.0 mg, t_R = 16.8 min), verruculogen (**2**, 7.0 mg, t_R = 15.5 min), and 12,13-dihydroxy-fumitremorgin C (**4,** 15 mg, t_R = 9.7 min).

Fumitremorgin B (**1**): white powder; ^{1}H- and ^{13}C-NMR data, see Table S1; HR-MS (ESI+) detected at *m/z* 462.2369, *cald.* for $[M - H_2O + H]^+$ $C_{27}H_{32}N_3O_5$: *m/z* 462.2387.

Verruculogen (**2**): white powder; ^{1}H- and ^{13}C-NMR data, see Table S2; HR-MS (ESI+) detected at *m/z* 494.2266, *cald*. for $[M - H_2O + H]^+$ $C_{27}H_{33}N_3O_7$: *m/z* 494.2285.

12,13-dihydroxy-fumitremorgin C (**4**): pale yellow powder; ^{1}H- and ^{13}C-NMR data, see Table S4; HR-MS (ESI+) detected at *m/z* 394.1757, *cald*. for $[M - H_2O + H]^+$ $C_{22}H_{24}N_3O_4$: *m/z* 394.1761.

Amino acid sequences of FtmOx1 with the N-terminal strep-tag

MGDRGPEFWSHPQFEKTVDSKPQLQRLAADADVDRMCRLLEEDGAFILKGLLPFDVVESFNRELDVQM
AIPPPKGERLLADKYPPHFKYVPNVATTCPTFRNTVLINPVIHAICEAYFQRTGDYWLSAAFLREIESGMP
AQPFHRDDATHPLMHYQPLEAPPVSLSVIFPLTEFTEENGATEVILGSHRWTEVGTPERDQAVLATMDP
GDVLIVRQRVVHAGGGNRTTAGKPRRVVLAYFNSVQLTPFETYRTMPREMVESMTVLGQRMLGWRTM
KPSDPNIVGINLIDDKRLENVLQLKAADSPALEVDLQGDHGLSA*

Structure determination and analysis

The FtmOx1•Co^{II} crystal shows identical space group and unit cell with previous reported FtmOx1•Fe^{II} structure (pdb entry 4Y5T), the FtmOx1•Co^{II}•αKG•**7** ternary complex crystal has the same space group type ($P2_1$) compared with FtmOx1•Fe^{II} structure, while having an expanded unit cell. A Cell Content Analysis suggested that in the FtmOx1•Co^{II}•αKG•**7** crystals, there are three dimers within one asymmetric unit, instead of having only one dimer as in the FtmOx1•Fe^{II} crystals. Such differences might be due to the small re-arrangement of the crystal lattice upon compound binding. The structure of the FtmOx1•Co^{II}•αKG•**7** complex was solved by molecular replacement using Phaser as implemented in the Phenix/CCP4 suite[1], using a model of PDB Entry 4Y5T (FtmOx1•Fe^{II} structure). The initial solution was refined using phenix.refine, and the resulting *Fo-Fc* omit map showed clear electron density for the substrate **7** located at the hydrophobic sub-pocket; the shape of the omit electron density fits quite well with compound **7**. The omit map located at the polar sub-pocket suggested the existence of αKG. The model was further improved using iterative cycles of manual model building in COOT[2], followed by computational refinement using phenix.refine[3-4]. After ligands were placed, potential sites of solvent molecules were identified by the automatic water-picking algorithm in COOT and phenix.refine. The positions of these automatically picked waters were checked manually during model building. The final model suggested a Real Space Correlation Coefficient (RSCC) ranging from 0.84 to 0.93 in each chain, indicating a good fit between compound **7** and electron density. Assuming the similar thermal factors for the ligand as surrounding residues, and the ligand occupancy is estimated to be in the

range of 0.81 to 0.86. Figures were generated with PyMOL (Schrödinger, LLC), and surface electrostatics were calculated with APBS[5].

Single-turnover enzymatic reaction of FtmOx1 and Y224F using fumitremorgin B (1) as substrate

These enzymatic reactions were performed in an anaerobic Coy chamber. For reactions of FtmOx1, The anaerobic reaction mixture (200 µl, in 100 mM Tris-HCl, pH 7.5) contained 140 µM fumitremorgin B (**1**), 140 µM FtmOx1 containing 126 µM Fe^{II}, 140 µM αKG, and 420 µM ascorbate (or w/o ascorbate). The reaction mixture was sealed and initiated by adding 200 µl of oxygen-saturated buffer (1.2 mM of oxygen) and incubated for 10 min at room temperature. The enzymatic reactions was quenched by adding 1 ml dichloromethane, the precipitated protein was removed by centrifugation at 13,000 g for 10 min, and the dichloromethane layer was carefully separated for further analysis. The reaction mixture was extracted once more using a second 1 ml volume of dichloromethane. The combined dichloromethane layers were concentrated by rotatory evaporation in vacuo, and the residue was re-dissolved in 1 ml of acetonitrile and subjected to LC-HR-MS(ESI) analysis on a Waters ACQUITY BEH C18 column (2.1 × 100 mm, 1.7 µm particles) with a flow rate of 0.35 ml/min (During 0–12 min, ACN was increased from 5% to 99% in 0.1% HCOOH-containing H_2O and then the column was eluted for 3 mins with 99% ACN in 0.1% HCOOH-containing H_2O). The reaction setup procejures of Y224F and LCMS analysis of enzymatic products were same to those of FtmOx1.

Single-turnover enzymatic conversion of 13-oxo-fumitremorgin B (7) by FtmOx1

The enzymatic reactions were performed in an anaerobic Coy chamber. For the single-turnover condition, the anaerobic reaction mixture (200 µl, in 100 mM Tris-HCl, pH 7.5) contained 140 µM 13-oxo-fumitremorgin B (**7**), 140 µM FtmOx1 containing 168 µM Fe^{II}, and 336 µM αKG. The reaction mixture was sealed and initiated by adding 200 µl of oxygen-saturated buffer (1.2 mM of oxygen) and incubated for 10 min at room temperature. The enzymatic reactions were quenched by adding 1 ml dichloromethane, the precipitated protein was removed by centrifugation at 13,000 *g* for 10 min, and the dichloromethane layer was carefully separated for further analysis. The reaction mixture was extracted once more using a second 1 ml volume of dichloromethane. The combined dichloromethane layers were concentrated by rotatory evaporation *in vacuo*, and the residue was re-dissolved in 1 ml of acetonitrile and subjected to LC-MS analysis on a C18 column (ACE Excel 5 C18, 4.6 × 250 mm, 5 µm) with a flow rate of 1.0 ml/min (During 0–15 min, ACN was increased from 10% to 99% in 0.1% HCOOH-containing H_2O and then the column was eluted for 5 mins with 99% ACN in 0.1% HCOOH-containing H_2O).

Single-turnover enzymatic conversion of verruculogen (2) by FtmOx1 and characterization of 13-oxo-verruculogen (3)

The enzymatic reactions were performed in an anaerobic Coy chamber. The anaerobic reaction mixture (400 µl, in 100 mM Tris-HCl, pH 7.5) contained 140 µM verruculogen (**2**), 140 µM FtmOx1 containing 168 µM Fe^{II}, and 168 µM αKG. The reaction mixture was sealed and initiated by adding

200 µl of oxygen-saturated buffer (1.2 mM of oxygen) and incubated for 30 min at room temperature. The resulting reaction mixtures contained a final concentration of 70 µM **2**, 70 µM FtmOx1 containing 84 µM Fe^{II}, and 84 µM αKG. The enzymatic reaction was quenched by adding 1 ml dichloromethane, the precipitated protein was removed by centrifugation at 13,000 *g* for 10 min, and the dichloromethane layer was carefully separated. The reaction mixture was extracted once more using a second 1 ml volume of dichloromethane. The combined dichloromethane layers were concentrated by rotatory evaporation, and the residue was re-dissolved in 100 µl of acetonitrile and subjected to LC-HR-MS(ESI) analysis on a Waters ACQUITY BEH C18 column (2.1 × 100 mm, 1.7 µm particles) with a flow rate of 0.35 ml/min (During 0–12 min, ACN was increased from 5% to 99% in 0.1% HCOOH-containing H_2O and then the column was eluted for 3 min with 99% ACN in 0.1% HCOOH-containing H_2O).

We synthesized the 13-oxo-verruculogen (**3**) and used it as standard in the LC-MS analysis mentioned above. To a solution of verruculogen (**2**, 5 mg) in acetone (2.5 ml) was added 2,3-Dichloro-5,6-dicyano-1,4-benzoquinone (DDQ; 98%; 120 mg) under an ice-water bath. After stirring for 8 hours, the reaction mixture was filtered by 0.22 µm membrane and analyzed by LC-MS. The reaction mixture was concentrated and redissolved in 1 ml MeOH. The sample was further purified by a semi-prep HPLC running with ACN-H_2O (During 0–15 min, ACN was increased from 10% to 99% in 0.1% HCOOH-containing H_2O and then the column was eluted for 5 mins with 99% ACN in 0.1% HCOOH-containing H_2O) at 4 ml/min using a C18 column (Titank, 10 × 250 mm) to obtain 13-oxo-verruculogen (**3**, 2.8 mg, t_R = 13.2 min).

13-oxo-verruculogen (**3**): pale-yellow powder; ^1H- and ^{13}C- NMR data, see Table S3; HR-MS (ESI+) detected at m/z 510.2210, *cald*. for $[M + H]^+$ $C_{27}H_{31}N_3O_7$: m/z 510.2234.

Decomposion of verruculogen (3) into verruculogen TR-2 (6) using excess ascorbate and Fe(II)

Verruculogen (**3**, 5 mg, 9.78 mmol) was dissolved in 300 µL DMSO and diluted with 3 mL Tris-HCl buffer (100 mM, pH 7.5), which was further added with sodium ascorbate (96.9 mg, 50 equiv.) and $FeSO_4 \cdot 7H_2O$ (13.6 mg, 5 equiv.) at room temperature. After stirring for 2 h, the reaction mixture was extracted with 5 ml of dichloromethane for three times, the combined dichloromethane layers were then concentrated by rotatory evaporation, and the residue was re-dissolved in 200 µl of acetonitrile. The sample was subjected to the semi-preparative RP-HPLC for purification, running with a C18 column (Titank, 10 × 250 mm, 5 µm) and eluted with ACN-H_2O (During 0–15 min, ACN was increased from 10% to 99% in 0.1% HCOOH-containing H_2O and then the column was eluted for 5 mins with 99% ACN in 0.1% HCOOH-containing H_2O) at 4 ml/min, to obtain verruculogen TR-2 (**5**, 0.6 mg, t_R = 8.2 min, 14% yeild).

verruculogen TR-2 (**6**): pale-yellow powder; ^1H- and ^{13}C-NMR data, see Table S6; HR-MS (ESI+) detected at m/z 412.1861, *cald*. for $[M - H_2O + H]^+$ $C_{22}H_{26}N_3O_5$: m/z 412.1867.

Supplementary schemes

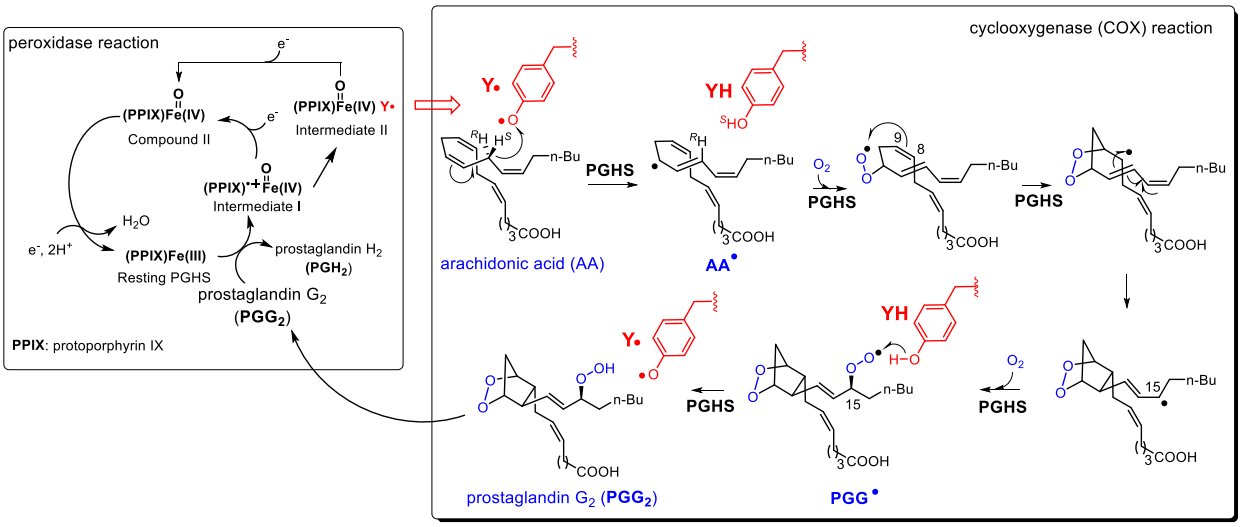

Scheme S1. Tyrosyl radical-based catalytic cycle of the proposed mechanism of prostaglandin H synthase (PGHS or COX).

COX catalyzed the conversion of arachidonic acid (AA) and two molecules of O_2 to prostaglandin endoperoxide G_2 (PGG_2), based on a branched-chain model[6-7].

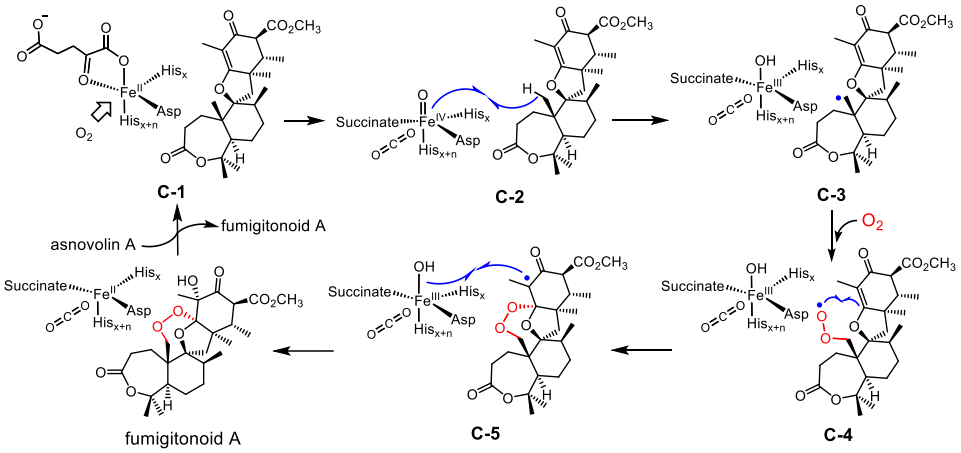

Scheme S2. Proposed mechanism of NvfI-catalyzed endoperoxidation.

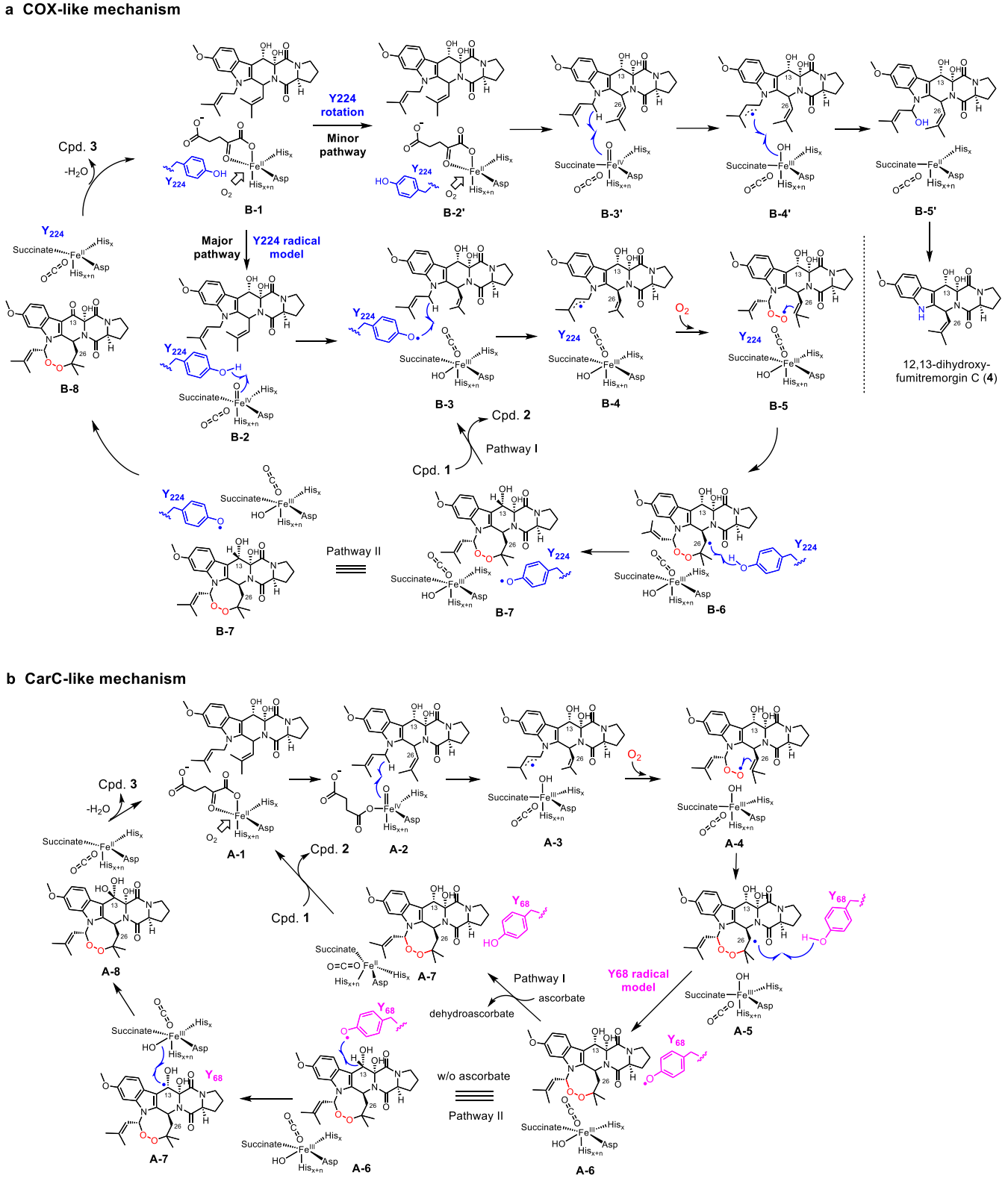

Scheme S3. The complete mechanistic models of COX-like and CarC-like proposed for FtmOx1-catalysis.

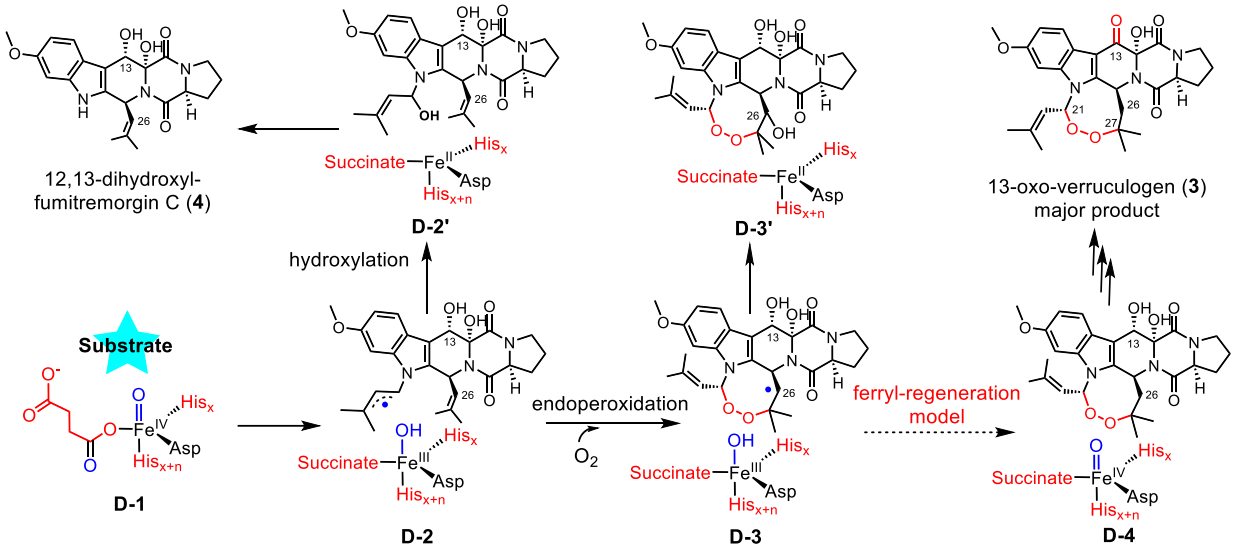

Scheme S4. The proposed ferryl-regeneration model from an undisclosed *Nature* reader.

Supplementary figures

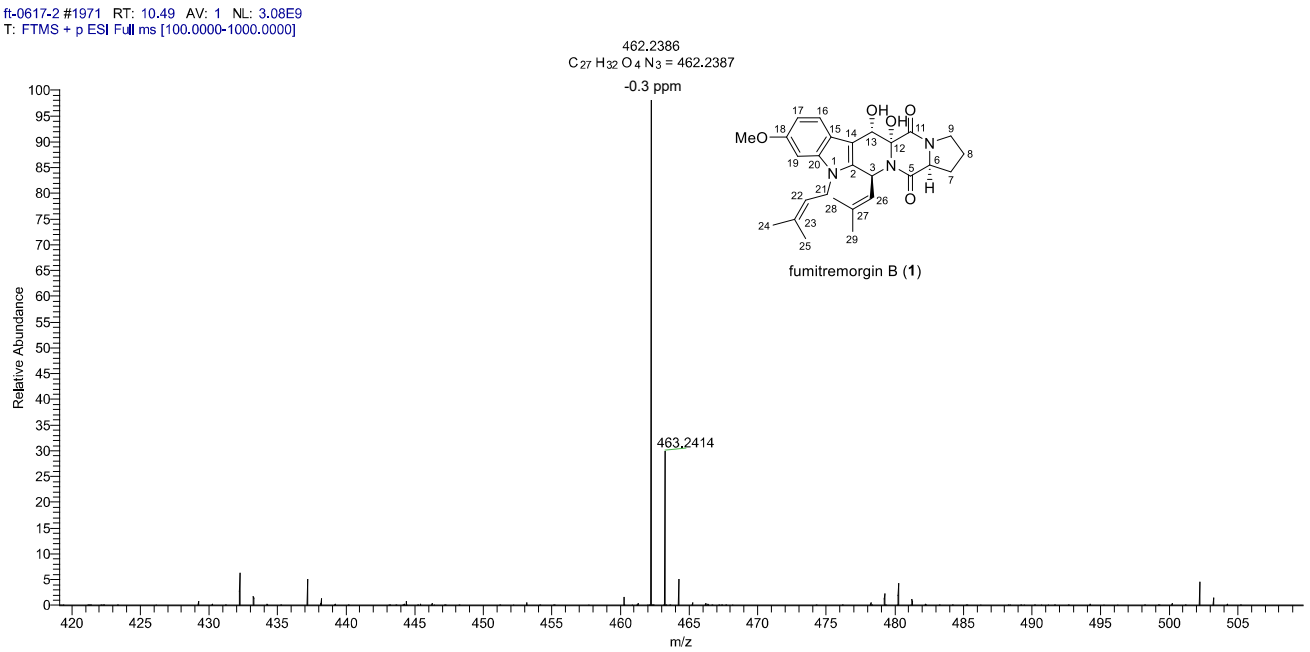

Figure S1a. HR-ESI-MS spectrum of fumitremorgin B (**1**).

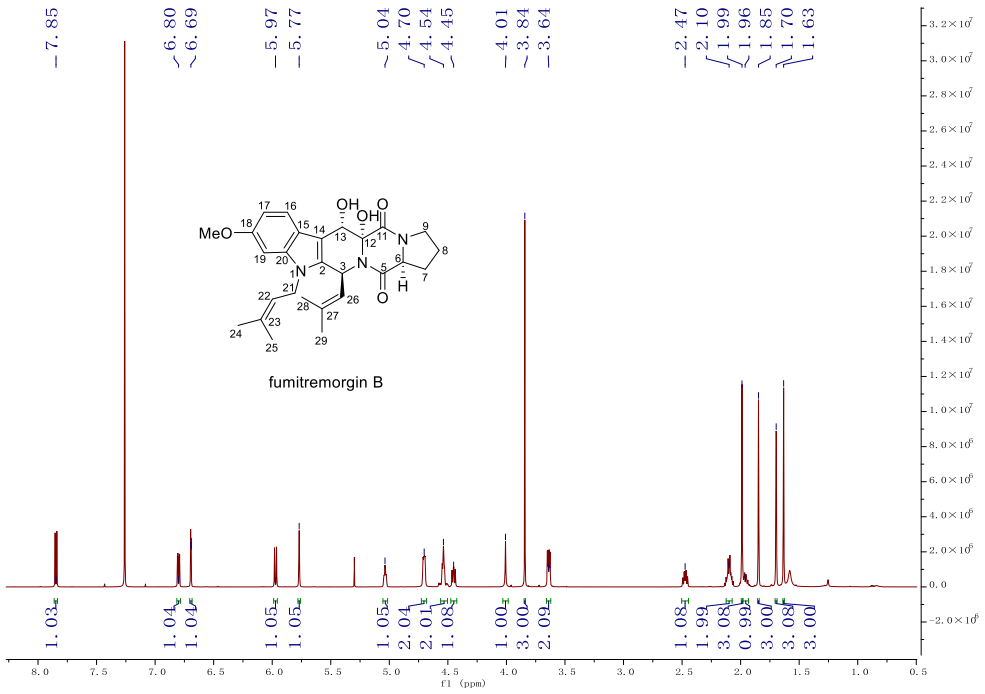

Figure S1b. ^{1}H NMR spectrum of fumitremorgin B (**1**) (600 MHz, $CDCl_3$-d_6).

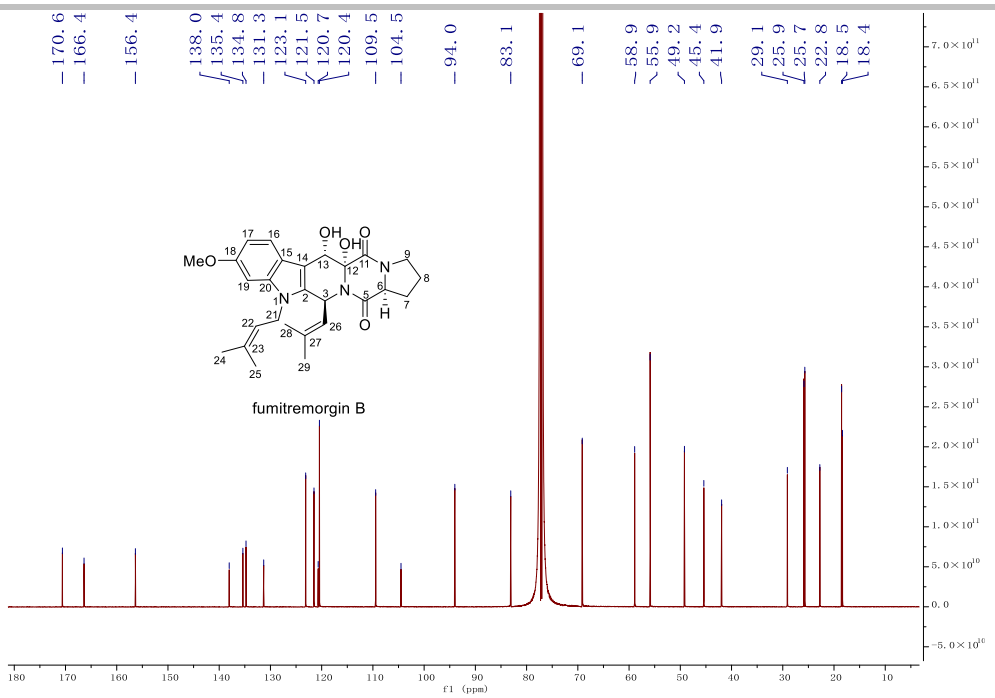

Figure S1c. ^{13}C NMR spectrum of fumitremorgin B (**1**) (150 MHz, $CDCl_3$-d_6).

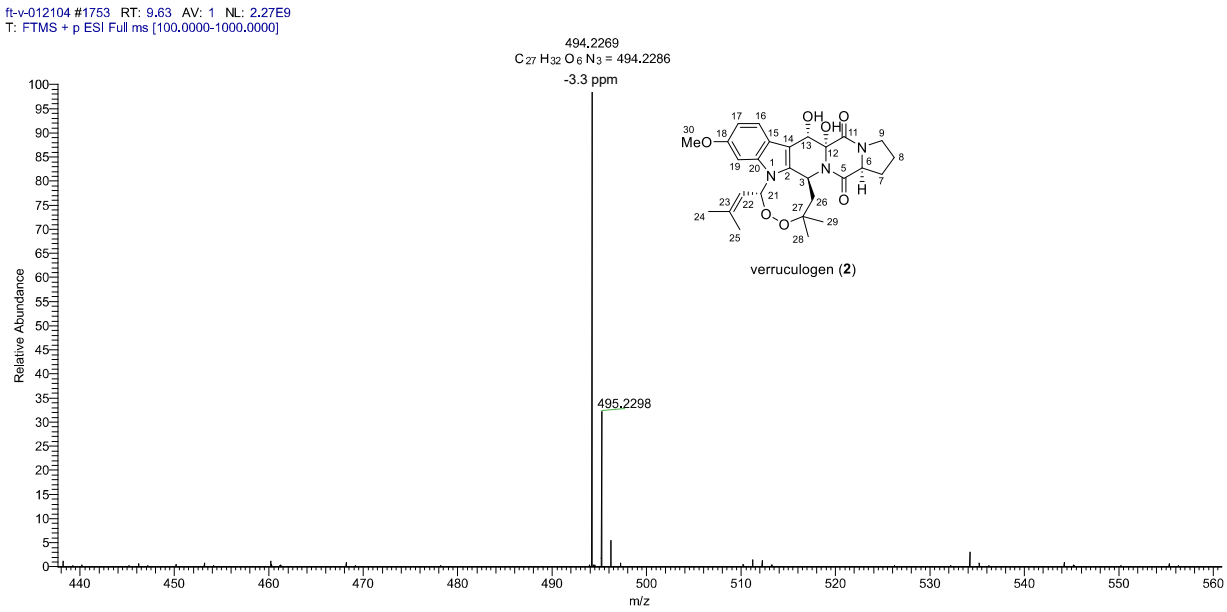

Figure S2a. HR-ESI-MS spectrum of verruculogen (**2**).

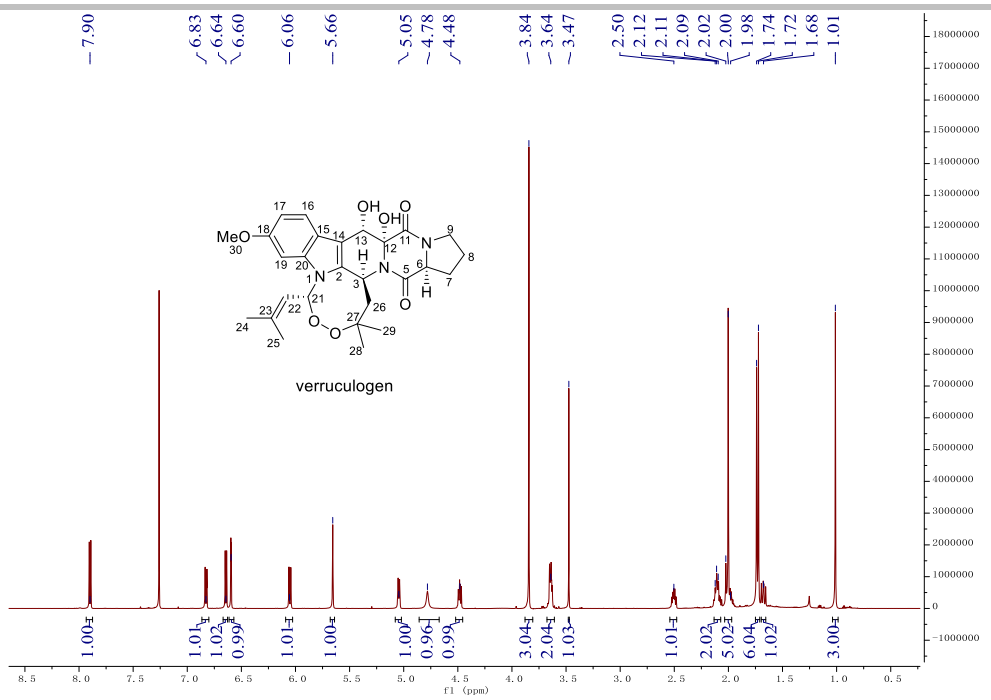

Figure S2b. ^{1}H NMR spectrum of verruculogen (**2**) (600 MHz, DMSO-d_6).

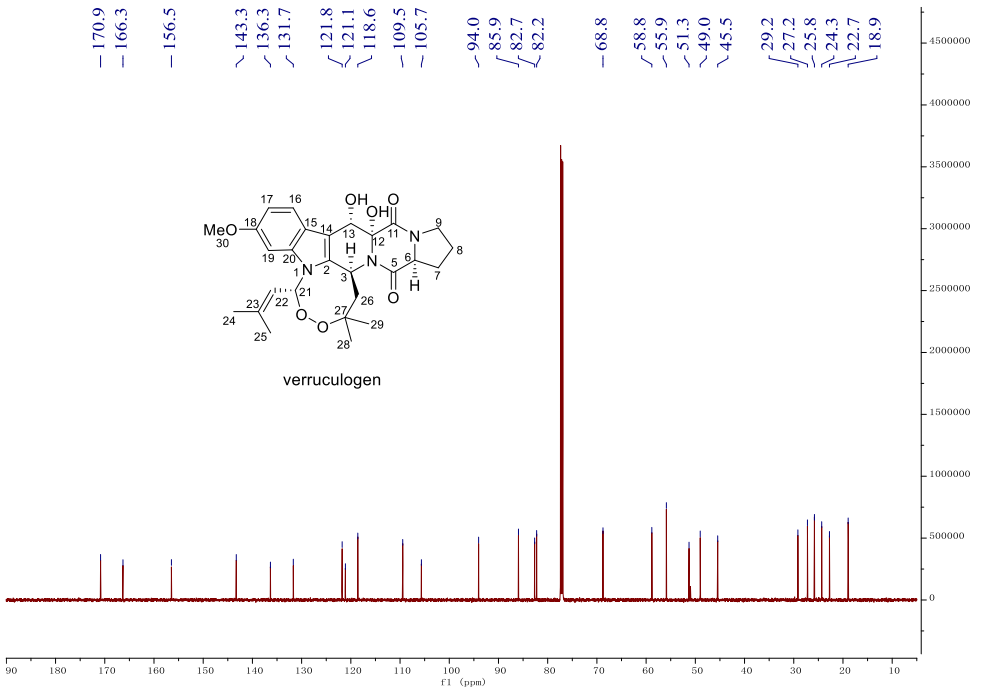

Figure S2c. ^{13}C NMR spectrum of verruculogen (**2**) (150 MHz, DMSO-d_6).

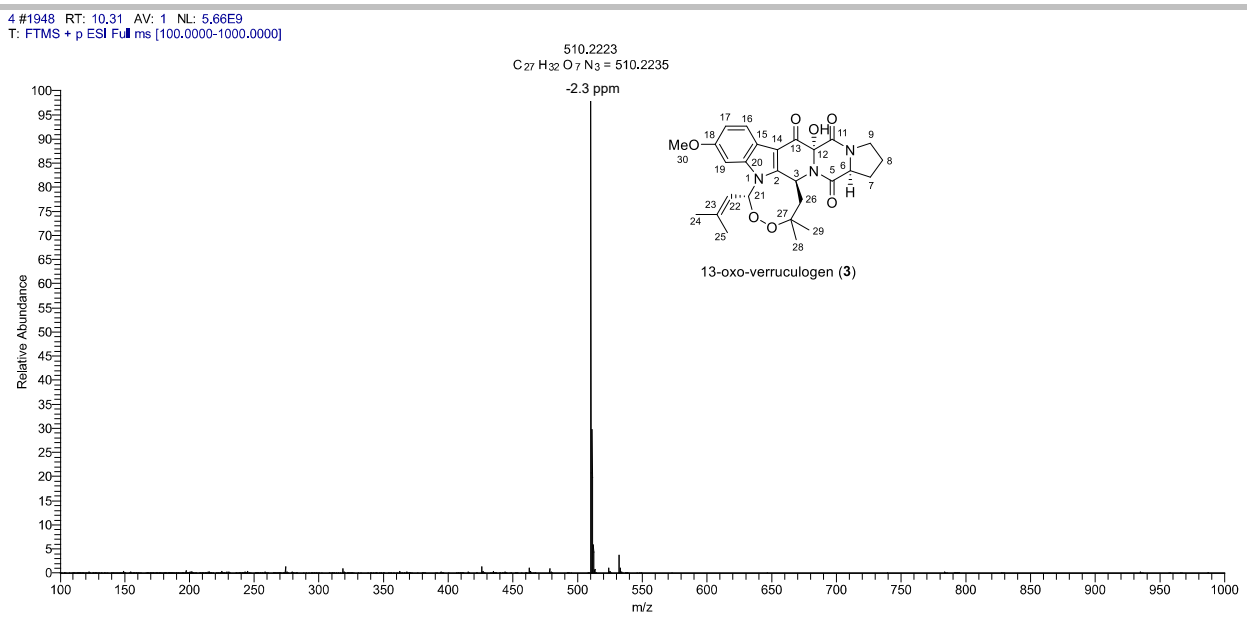

Figure S3a. HR-ESI-MS spectrum of 13-oxo-verruculogen (**3**).

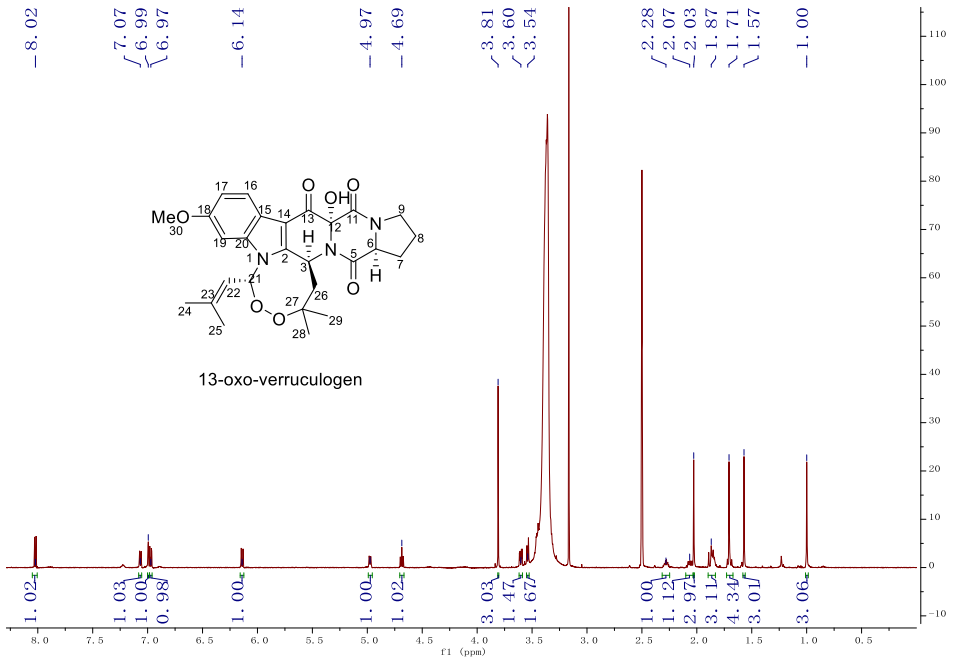

Figure S3b. ^{1}H NMR spectrum of 13-oxo-verruculogen (**3**) (600 MHz, DMSO-d_6).

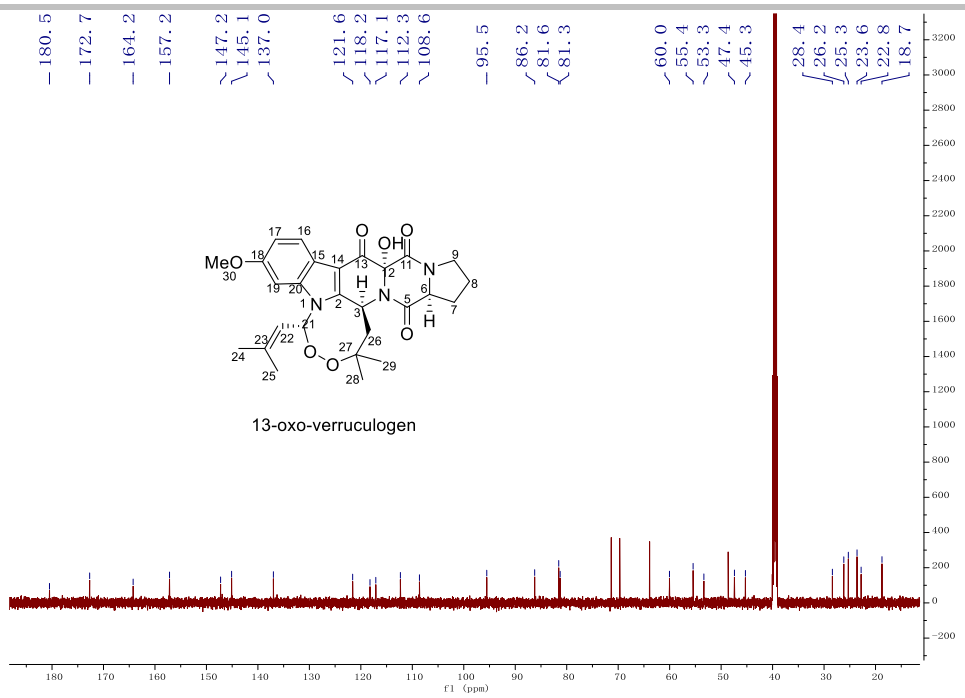

Figure S3c. ^{13}C NMR spectrum of 13-oxo-verruculogen (**3**) (150 MHz, DMSO-d_6).

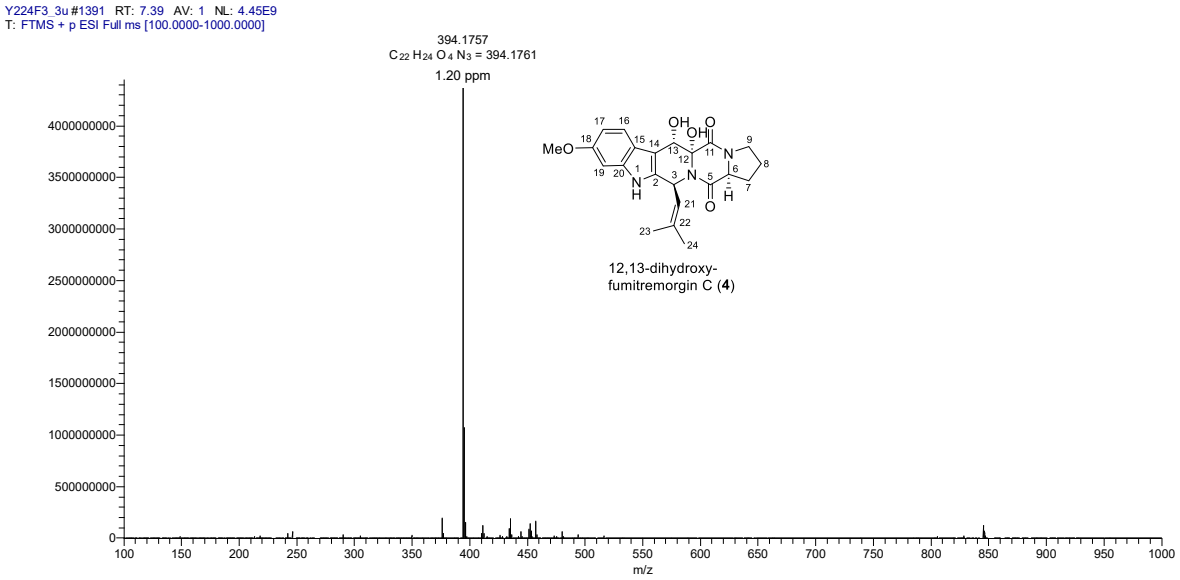

Figure S4a. HR-ESI-MS spectrum of 12, 13-dihydroxy-fumitremorgin C (**4**).

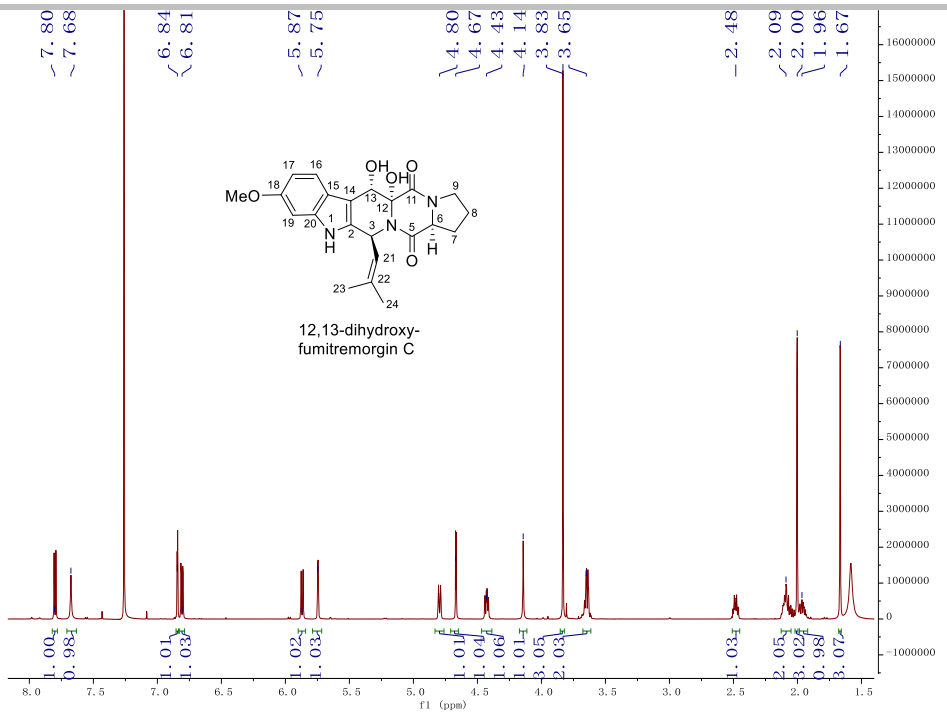

Figure S4b. ^{1}H NMR spectrum of 12,13-dihydroxy-fumitremorgin C (**4**). (600 MHz, $CDCl_3$).

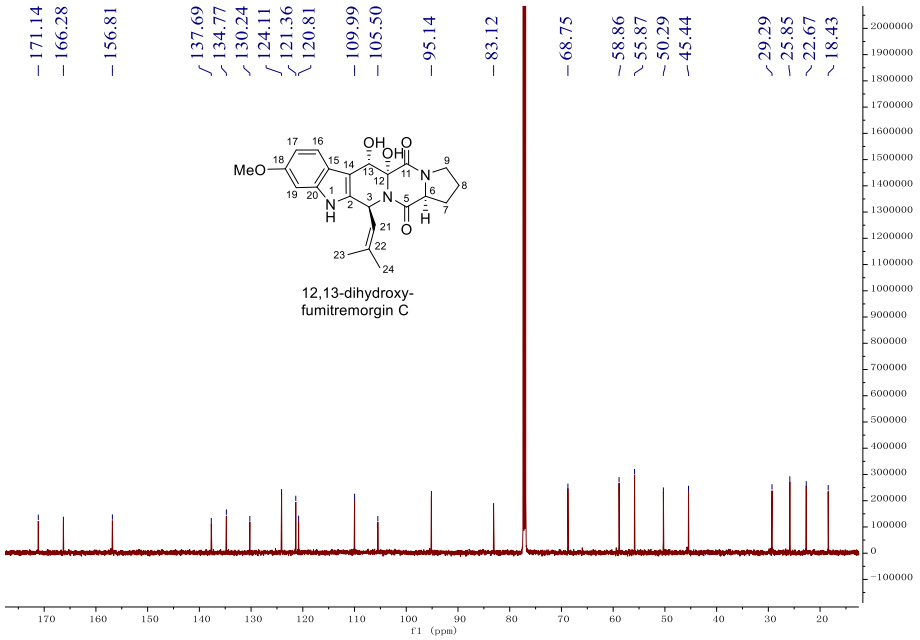

Figure S4c. ^{13}C NMR spectrum of 12,13-dihydroxy-fumitremorgin C (**4**). (150 MHz, $CDCl_3$).

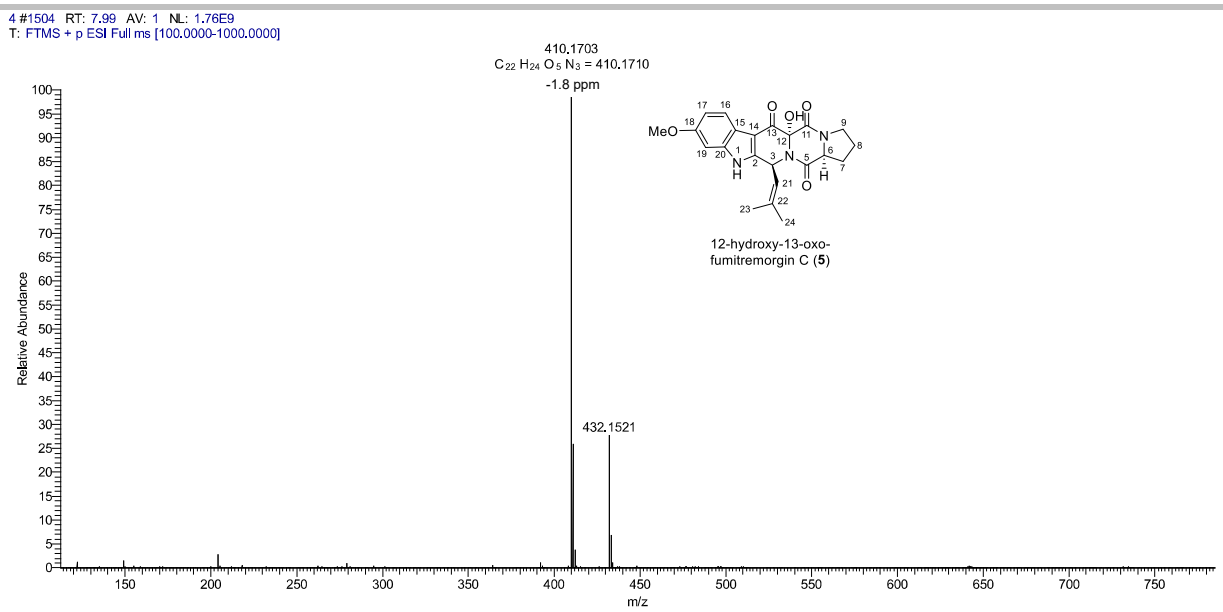

Figure S5a. HR-ESI-MS spectrum of 12-hydroxy-13-oxo-fumitremorgin C (**5**).

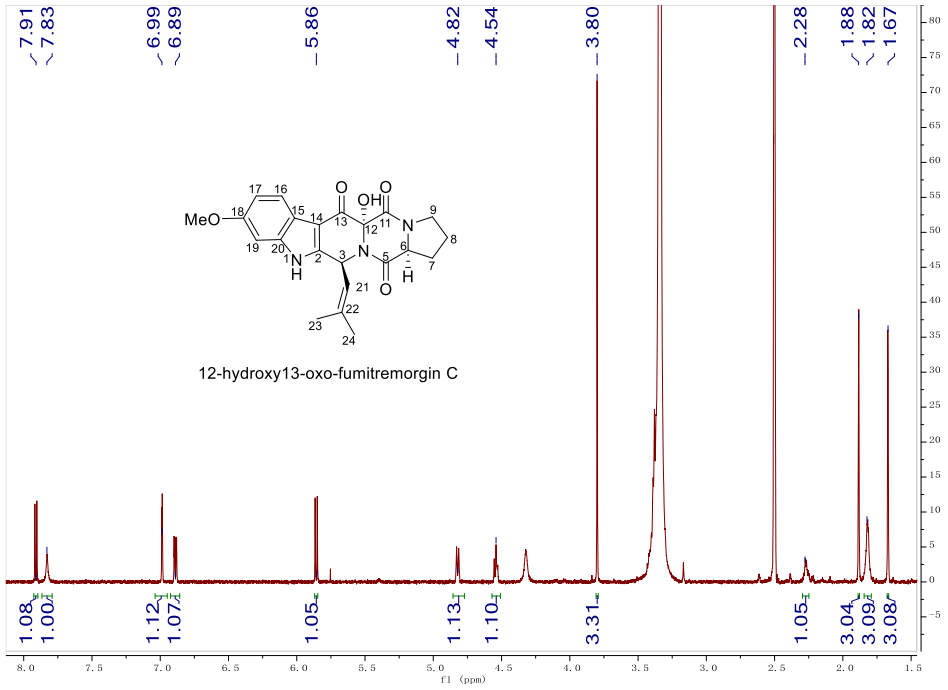

Figure S5b. ^{1}H NMR spectrum of 12-hydroxy-13-oxo-fumitremorgin C (**5**) (600 MHz, DMSO-d_6).

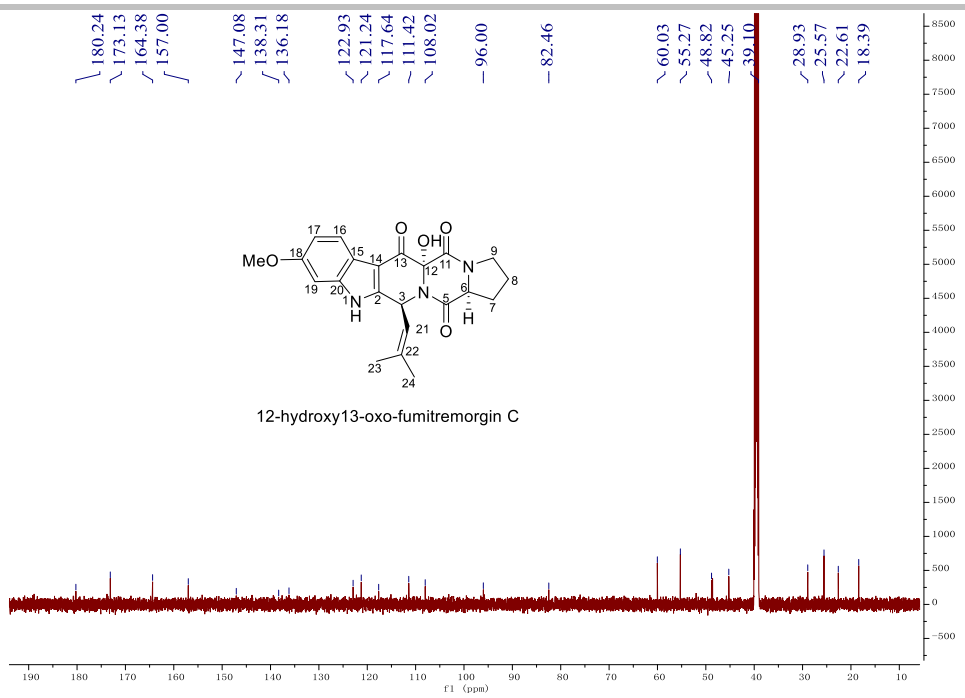

Figure S5c. ^{13}C NMR spectrum of 12-hydroxy-13-oxo-fumitremorgin C (**5**) (150 MHz, DMSO-d_6).

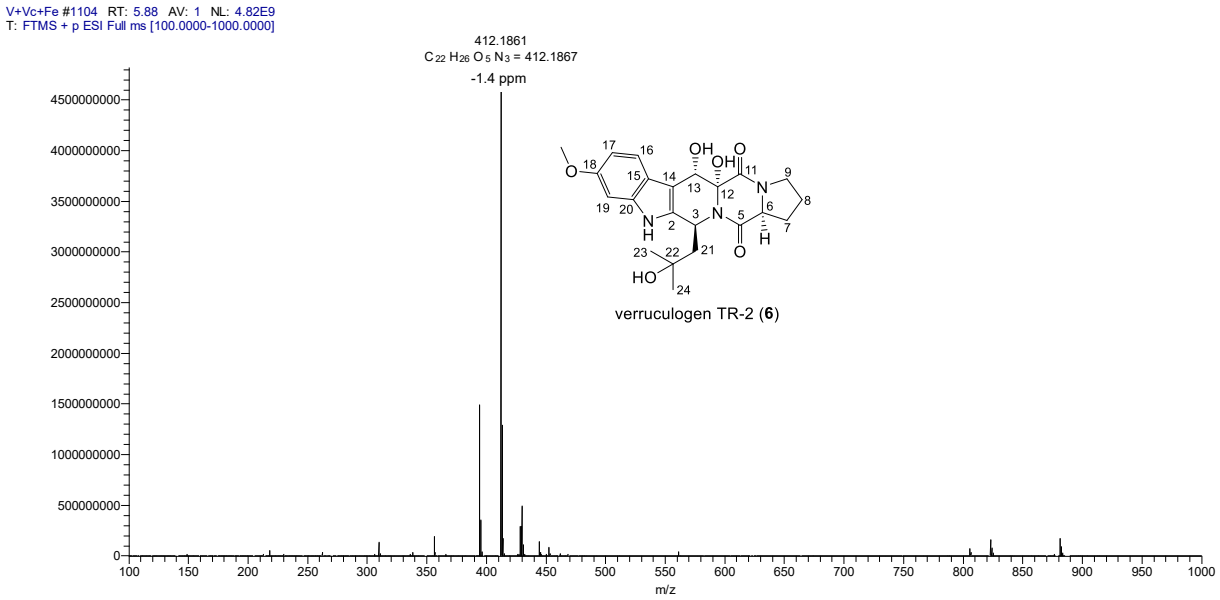

Figure S6a. HR-ESI-MS spectrum of verruculogen TR-2 (**6**).

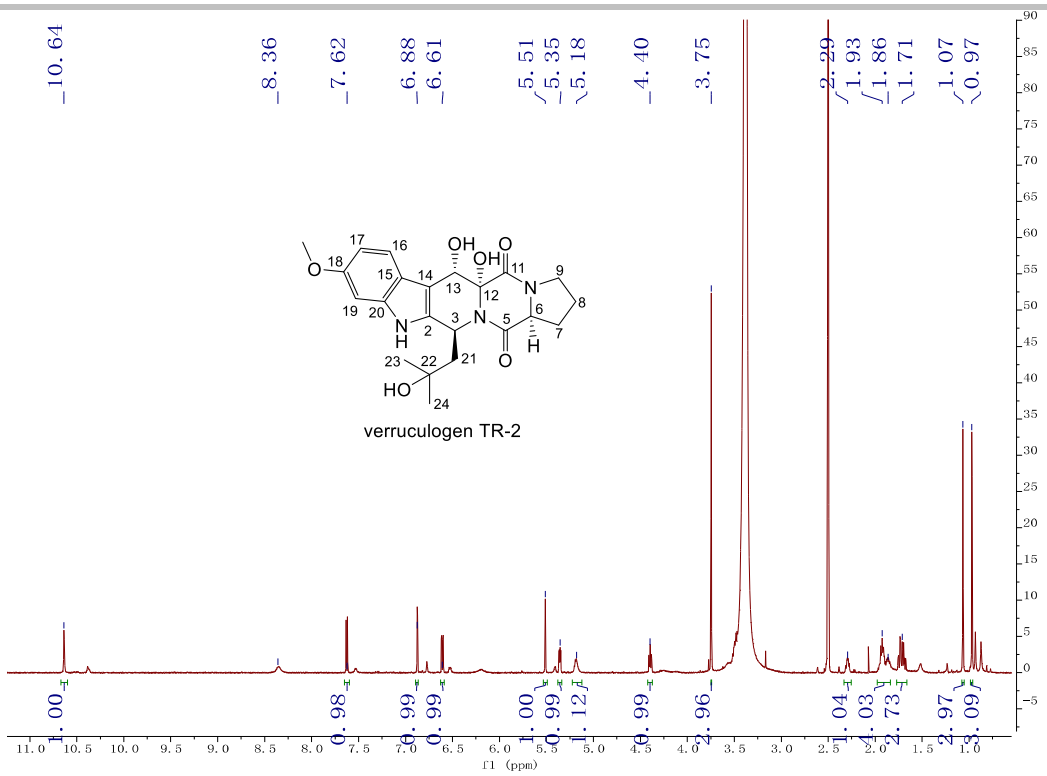

Figure S6b. ^{1}H NMR spectrum of verruculogen TR-2 (**6**) (600 MHz, DMSO-d_6).

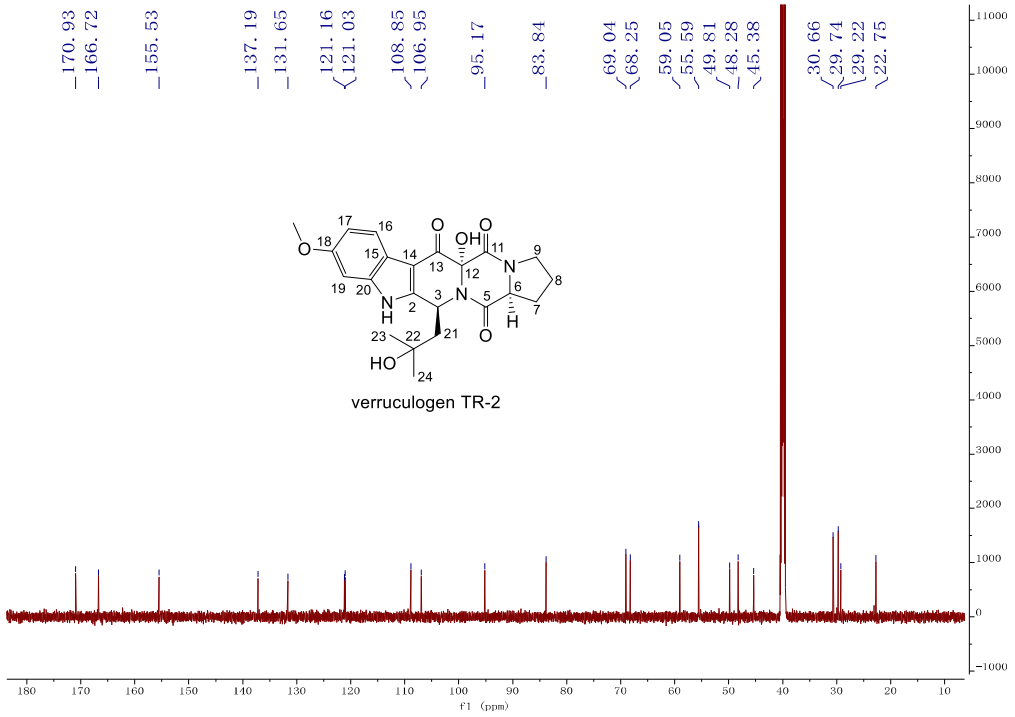

Figure S6c. ^{13}C NMR spectrum of verruculogen TR-2 (**6**) (150 MHz, DMSO-d_6).

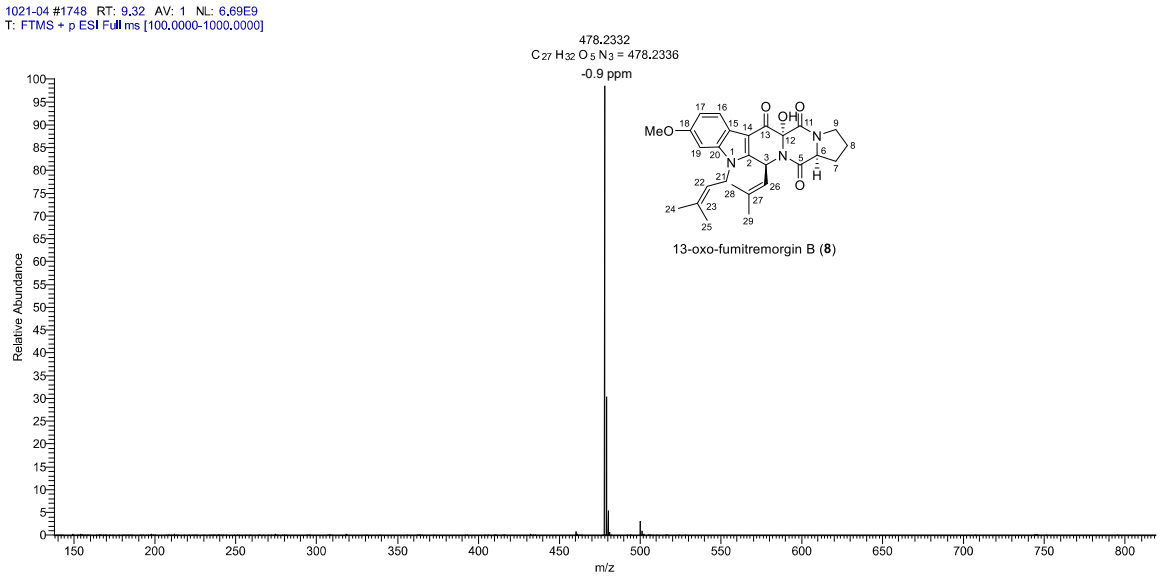

Figure S7a. HR-ESI-MS spectrum of 13-oxo-fumitremorgin B (**7**).

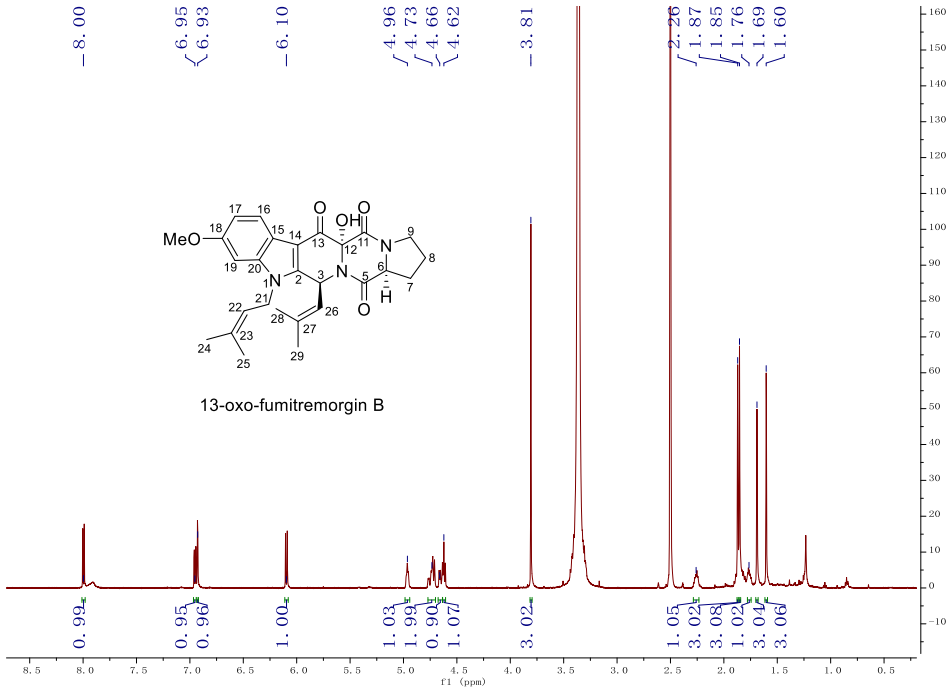

Figure S7b. ^{1}H NMR spectrum of 13-oxo-fumitremorgin B (**7**) (600 MHz, DMSO-d_6).

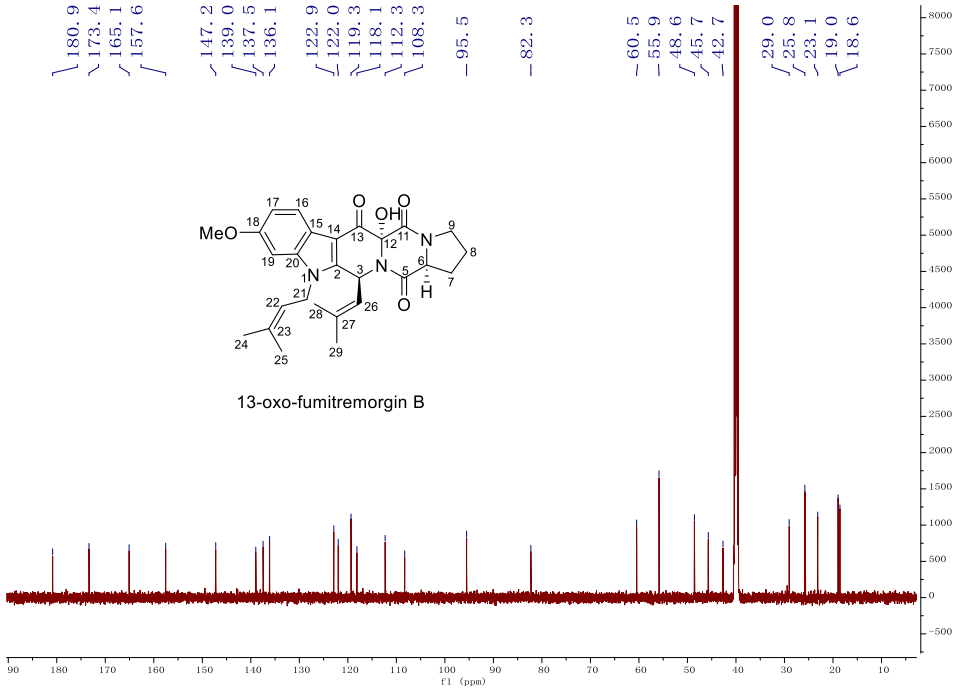

Figure S7c. ^{13}C NMR spectrum of 13-oxo-fumitremorgin B (**7**) (150 MHz, DMSO-d_6).

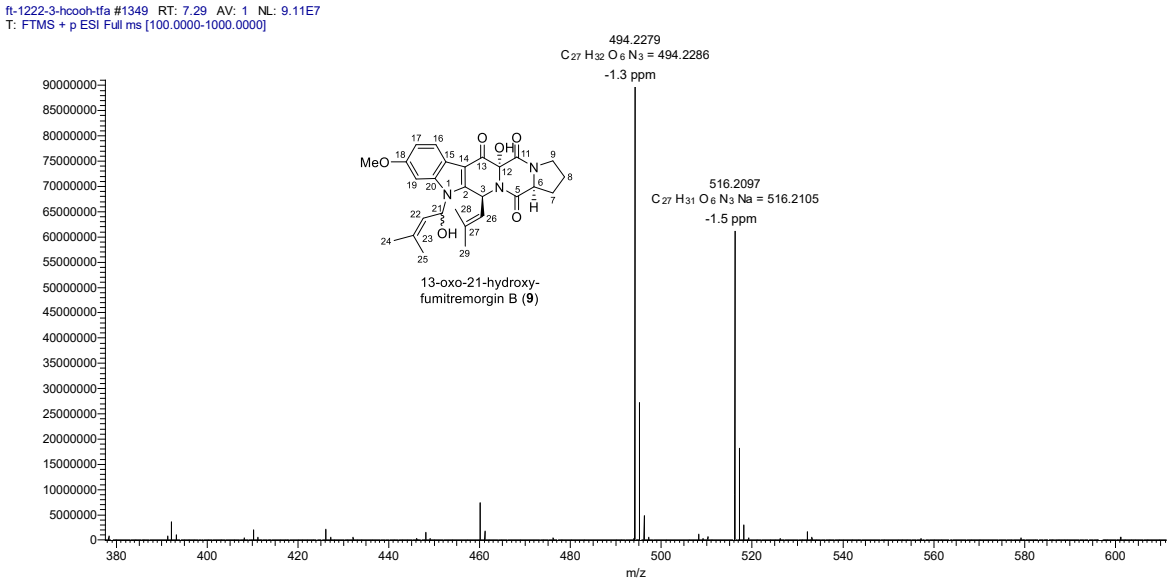

Figure S8a. HR-ESI-MS spectrum of 13-oxo-21-hydroxy-fumitremorgin B (**8**).

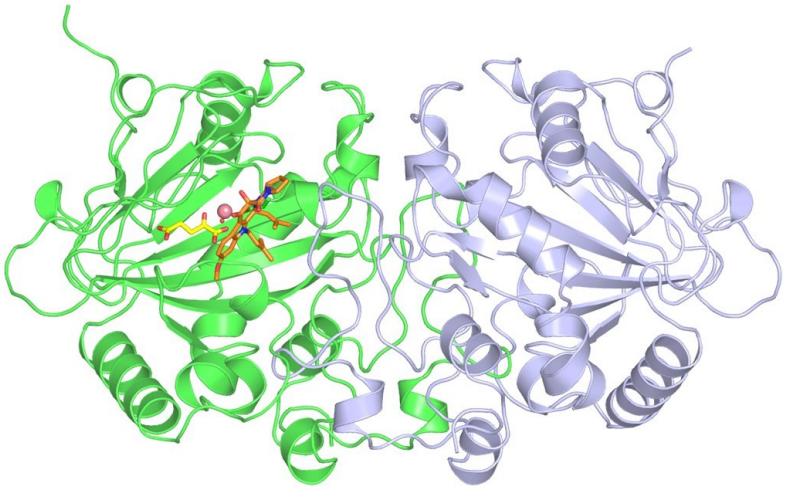

Figure S9. Overall architecture of the FtmOx1•Co^{II}•αKG•**7** ternary complex.

Monomers of FtmOx1 are colored in green and light blue, respectively. The cobalt is shown as a pink sphere, and the substrates are shown as orange (**7**) and yellow (αKG) sticks.

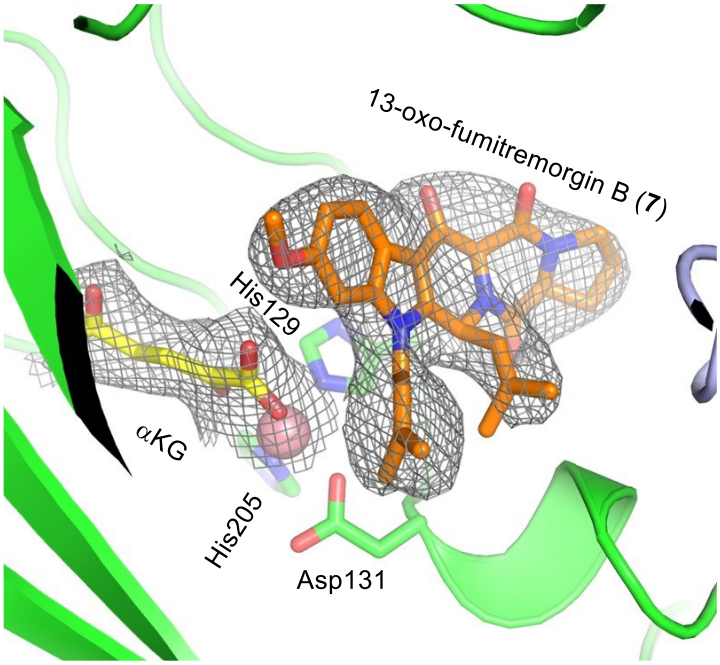

Figure S10. Composite omit map (*2mFo-DFc*) showing substrate 13-oxo-fumitremorgin B (**7**) and αKG at the FtmOx1 active site.

The map was generated by phenix using simple refinement after omitting each region. The electron density around each compound is shown in grey mesh, with the contour level at 1.0 rmsd. The residues coordinating with the metallo-center are shown as stick.

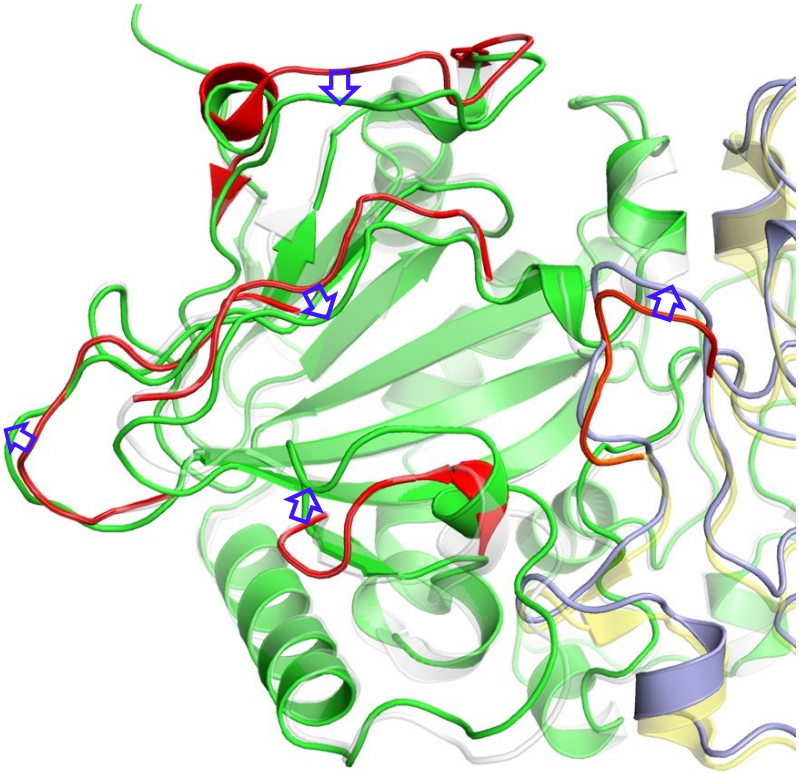

Figure S11. Superimposition of the FtmOx1 ternary structure with FtmOx1•Fe^{II}•αKG structure (pdb entry 4Y5S).

The FtmOx1•Fe^{II}•αKG complex structure is shown in white and yellow with 50% transparency. The regions of FtmOx1•Fe^{II}•αKG complex structure that had been re-arranged upon substrate **7** binding were colored in red with arrows to show the moving directions.

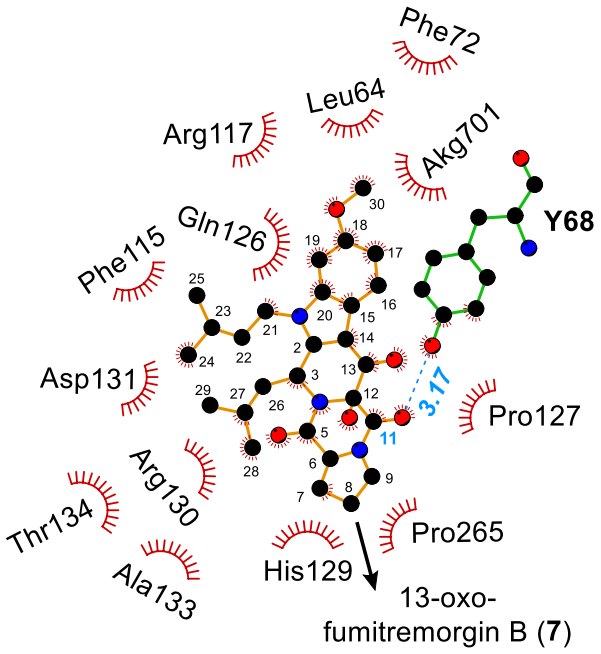

Figure S12. Interaction diagram between compound **7** and FtmOx1. The figure was prepared using Ligplot.

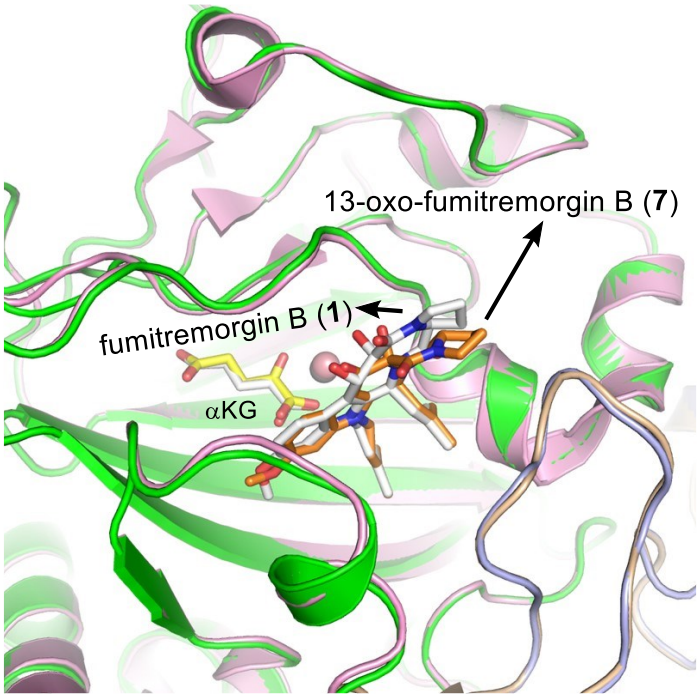

Figure S13. Superimposition of the FtmOx1•Co^{II}•αKG•**7** complex structure with the FtmOx1•Fe^{II}•αKG•**1** complex structure.

The FtmOx1•Co^{II}•αKG•**7** complex structure is shown in green and blue, while the FtmOx1•Fe^{II}•αKG•**1** complex structure is shown in white and wheat.

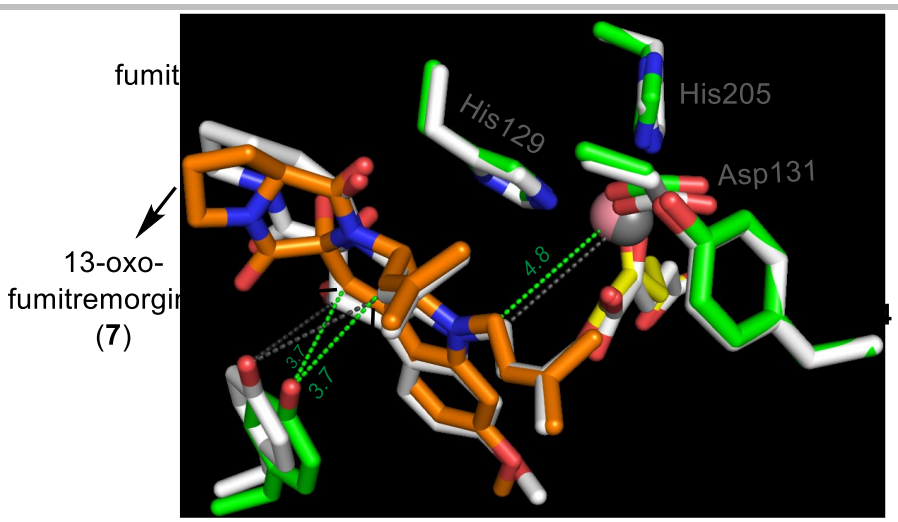

Figure S14. Active site comparison between the FtmOx1•Co^{II}•αKG•**7** complex and the FtmOx1•Fe^{II}•αKG•**1** complex (pdb entry 7ETK).

(The opposite view complementary to Figure 4a in the main text)

Supplementary Tables

Table S1. ^{1}H and ^{13}C-NMR data of fumitremorgin B (**1**).

Pos.	δ_H[a], mult (*J* in Hz)	δ_C[b], type
2		131.3, C
3	5.97, d (10.0)	49.2, CH
5		166.4, C
6	4.45, dd (10.1, 6.9)	58.9, CH
7a	1.94, m, overlapped	29.1, CH_2
7b	2.47, m	
8	2.10, m	22.8, CH_2
9	3.64, dd (9.2, 4.5)	45.4, CH_2
11		170.6, C
12		83.1, C
12-OH	4.01, brs	
13	5.77, brs	69.1, CH
13-OH	4.70, m	
14		104.5, C
15		120.4, C
16	7.85, d (8.7)	121.5, CH
17	6.80, dd (8.7, 2.2)	109.5, CH
18		156.4, C
19	6.69, d (2.2)	94.0, CH
20		138.0, C
21	4.54, m	41.9, CH_2
22	5.04, m	120.7, CH
23		134.8, C
24	1.85, s	18.4, CH_3
25	1.70, s	25.9, CH_3
26	4.70, m, overlapped	123.1, CH
27		135.4, C
28	1.99, s	18.5, CH_3
29	1.63, s	25.7, CH_3
30	3.84, s	55.9, CH_3

[a]Recorded at 600 MHz in $CDCl_3$. [b]Recorded at 150 MHz in $CDCl_3$.

Table S2. ^{1}H- and ^{13}C-NMR data of verruculogen (**2**).

Pos.	δ_H[a] mult (*J* in Hz)	δ_C[b], type
2		131.7, C
3	6.06, d (10.2)	49.0, CH
5		170.9, C
6	4.48, dd (10.0, 7.2)	58.8, CH
7a	2.50, m	29.2, CH_2
7b	2.11, m, overlapped	
8a	2.12, m, overlapped	22.7, CH_2
8b	1.98, m	
9	3.64, m	45.5, CH_2
11		166.3, C
12		82.7, C
13	5.66, s	68.8, CH
14		105.7, C
15		121.1, C
16	7.90, d (8.6)	121.8, CH
17	6.83, dd (8.6, 2.2)	109.5, CH
18		156.5, C
19	6.60, d (2.2)	94.0, CH
20		136.3, C
21	6.64, d (8.2)	85.9, CH
22	5.05, m	118.6, CH
23		143.3, C
24	2.00, brs	18.9, CH_3
25	1.74, brs	25.8, CH_3
26a	2.02, d (13.4)	51.3, CH_2
26b	1.68, dd (13.5, 10.2)	
27		82.2, C
28	1.01, s	27.2, CH_3
29	1.72, s	24.3, CH_3
30	3.84, s	55.9, CH_3
13-OH	4.78, brs	

[a]Recorded at 600 MHz in $CDCl_3$. [b]Recorded at 150 MHz in $CDCl_3$.

Table S3. ^{1}H- and ^{13}C-NMR data of 13-oxo-verruculogen (**3**).

Pos.	δ_H[a] mult (*J* in Hz)	δ_C[b], type
2		147.2, C
3	6.14, d (9.8)	47.4, CH
5		172.7, C
6	4.69, t (8.3)	60.0, CH
7a	2.28, m	28.4, CH_2
7b	2.07, m	
8	1.76, m	22.8, CH_2
9a	3.60, m, overlapped	45.3, CH_2
9b	3.54, m, overlapped	
11		164.2, C
12		81.3, C
13		180.4, C
14		108.6, C
15		118.2, C
16	8.02, d (8.6)	121.6, CH
17	6.97, dd (8.6, 2.2)	112.3, CH
18		157.2, C
19	6.99, d (2.2)	95.5, CH
20		137.0, C
21	7.08, d (8.4)	86.2, CH
22	4.97, d (8.4)	117.1, CH
23		145.1, C
24	2.03, s	18.7, CH_3
25	1.71, s	25.3, CH_3
26a	1.87, m, overlapped	53.3, CH_2
26b	1.71, m, overlapped	
27		81.6, C
28	1.00, s	26.2, CH_3
29	1.57, s	23.6, CH_3
30	3.81, s	55.4, CH_3

[a]Recorded at 600 MHz in DMSO-d_6. [b]Recorded at 150 MHz in DMSO-d_6.

Table S4. ^{1}H- and ^{13}C-NMR data of 12,13-dihydroxy-fumitremorgin C (**4**).

Pos.	δ_H[a] mult (*J* in Hz)	δ_C[b], type
1-NH	7.68, s	
2		130.2, C
3	5.87, dd (9.6, 0.9)	50.3, CH
5		171.1, C
6	4.43, dd (10.2, 6.8)	58.9, CH
7a	2.48, m	29.3, CH_2
7b	2.00, m	
8	2.09, m	22.7, CH_2
9	3.65, m	45.6, CH_2
11		166.3, C
12		83.1, C
13	5.75, s	68.8, CH
14		105.5, C
15		120.8, C
16	7.80, d (8.7)	121.4, CH
17	6.81, d (8.7, 2.1)	110.0, CH
18		156.8, C
19	6.84, d (2.1)	95.1, CH
20		137.7, C
21	4.80, d (9.6)	124.1, CH
22		134.8, C
23	1.67, s	25.8, CH_3
24	2.00, s	18.4, CH_3
25	3.83, s	55.9, CH_3

[a]Recorded at 600 MHz in $CDCl_3$. [b]Recorded at 150 MHz in $CDCl_3$.

Table S5. ^{1}H- and ^{13}C-NMR data of 12-hydroxy-13-oxo-fumitremorgin C (**5**).

Pos.	δ_H[a] mult (*J* in Hz)	δ_C[b], type
2		147.1, C
3	5.86, d (9.3)	48.8, CH
5		173.1, C
6	4.54, t (7.8)	60.0, CH
7a	2.28, m	28.9, CH_2
7b	1.82, m, overlapped	
8	1.82, m, overlapped	22.6, CH_2
9a	3.42, m, overlapped	45.3, CH_2
9b	3.36, m, overlapped	
11		164.4, C
12		82.5, C
12-OH	7.83, brs	
13		180.2, C
14		108.0, C
15		117.6, C
16	7.91, d (8.4)	121.2, CH
17	6.89, dd (8.4, 2.3)	111.4, CH
18		157.0, C
19	6.99, d (2.3)	96.0, CH
20		138.3, C
21	4.82, d (9.1)	122.9, CH
22		136.2, C
23	1.67, d (0.9)	25.6, CH_3
24	1.88, d (0.9)	18.4, CH_3
25	3.80, s	55.3, CH_3

[a]Recorded at 600 MHz in DMSO-d_6. [b]Recorded at 150 MHz in DMSO-d_6.

Table S6. ^{1}H- and ^{13}C-NMR data of verruculogen TR-2 (**6**).

Pos.	δ_H[a] mult (*J* in Hz)	δ_C[b], type
1-NH	10.64, s	
2		137.2, C
3	5.36, dd (8.2, 3.9)	49.8, CH
5		170.9, C
6	4.40, t (7.8)	59.1, CH
7a	1.93, m	29.7, CH_2
7b	1.87, m	
8	2.73, m	22.8, CH_2
9	3.51, m (overlapped)	45.4, CH_2
11		166.7, C
12		83.8, C
12-OH	8.36, brs	
13		69.0, C
13-OH	5.50, s	
14		107.0, C
15		121.0, C
16	7.62, d (8.7)	121.2, C
17	6.61, dd (8.7, 2.3)	108.9, CH
18		155.5, C
19	6.88, d (2.3)	95.2, CH
20		131.7, C
21a	2.29, m	48.3, CH_2
21b	1.93, m	
22		68.3, C
22-OH	6.19, brs	
23	0.97, s	29.2, CH_3
24	1.07, s	30.7, CH_3
25	3.75, s	55.6, CH_3

[a]Recorded at 600 MHz in DMSO-d_6. [b]Recorded at 150 MHz in DMSO-d_6.

Table S7. ^{1}H- and ^{13}C-NMR data of 13-oxo-fumitremorgin B (**7**).

Pos.	δ_H[a] mult (*J* in Hz)	δ_C[b], type
2		147.2, C
3	6.10, d (9.8)	48.6, CH
5		165.1, C
6	4.73, m	60.5, CH
7	2.26, m	29.0, CH_2
8a	1.85, m	23.1, CH_2
8b	1.87, m, overlapped	
9	3.45, m	45.7, CH_2
11		173.4, C
12		82.3, C
13		180.9, C
14		108.3, C
15		118.1, C
16	8.00, d (8.6)	122.9, CH
17	6.95, dd (8.6, 2.2)	112.3, CH
18		157.6, C
19	6.93, d (2.2)	95.5, CH
20		139.0, C
21a	4.62, m	42.7, CH_2
21b	4.66, m	
22	4.96, m	119.3, CH
23		136.1, C
24	1.85, s	18.6, CH_3
25	1.69, s	25.8, CH_3
26	4.73, d (9.6)	122.0, CH
27		137.5, C
28	1.87, s	19.0, CH_3
29	1.60, s	25.7, CH_3
30	3.81, s	55.9, CH_3

[a]Recorded at 600 MHz in DMSO-d_6. [b]Recorded at 150 MHz in DMSO-d_6.

Table S8. Crystallographic data collection and refinement statistics for the FtmOx1•Co^{II}•αKG•**7** ternary complex.

Data Collection	
Wavelength (Å)	0.97852
Resolution range (Å)	30.00 - 2.87 (2.92 – 2.87)
Space group	P 1 2_1 1
Unit cell a, b, c (Å) β (°)	104.05 85.44 160.77 108.84
Unique reflections	60482 (2949)
Multiplicity	6.4 (6.3)
Completeness (%)	98.5 (97.6)
Mean I/sigma(I)	13.39 (2.44)
$CC_{1/2}$	0.980 (0.838)
R_{sym}	0.140 (0.608)
Refinement	
R_{work}	0.1608 (0.2161)
R_{free}	0.2110 (0.2601)
Number of non-hydrogen atoms	14026
macromolecules	13587
ligands	302
water	137
Protein residues	1706
RMS bonds (Å)	0.005
RMS angles (°)	0.794
Ramachandran favored (%)	98.06
Ramachandran outliers (%)	0
Average B-factor ($Å^2$)	52.77
macromolecules	52.76
ligands	58.19
solvent	42.23
[1]Statistics for the highest-resolution shell are shown in parentheses.	
[2] R_{free} is calculated with 5% of the data randomly omitted from refinement.	

References

(1) McCoy, A. J.; Grosse-Kunstleve, R. W.; Adams, P. D.; Winn, M. D.; Storoni, L. C.; Read, R. J., Phaser crystallographic software. *J. Appl. Crystallogr.* **2007,** *40*, 658–674.

(2) Emsley, P.; Lohkamp, B.; Scott, W. G.; Cowtan, K., Features and development of Coot. *Acta. Crystallogr. D. Biol. Crystallogr.* **2010,** *66*, 486–501.

(3) Afonine, P. V.; Grosse-Kunstleve, R. W.; Echols, N.; Headd, J. J.; Moriarty, N. W.; Mustyakimov, M.; Terwilliger, T. C.; Urzhumtsev, A.; Zwart, P. H.; Adams, P. D., Towards automated crystallographic structure refinement with phenix.refine. *Acta. Crystallogr. D. Biol. Crystallogr.* **2012,** *68*, 352–67.

(4) Liebschner, D.; Afonine, P. V.; Baker, M. L.; Bunkoczi, G.; Chen, V. B.; Croll, T. I.; Hintze, B.; Hung, L.-W.; Jain, S.; McCoy, A. J.; Moriarty, N. W.; Oeffner, R. D.; Poon, B. K.; Prisant, M. G.; Read, R. J.; Richardson, J. S.; Richardson, D. C.; Sammito, M. D.; Sobolev, O. V.; Stockwell, D. H.; Terwilliger, T. C.; Urzhumtsev, A. G.; Videau, L. L.; Williams, C. J.; Adams, P. D., Macromolecular structure determination using X-rays, neutrons and electrons: recent developments in Phenix. *Acta. Crystallogr. D.* **2019,** *75* (10), 861–877.

(5) Baker, N. A.; Sept, D.; Joseph, S.; Holst, M. J.; McCammon, J. A., Electrostatics of nanosystems: application to microtubules and the ribosome. *Proc. Natl. Acad. Sci. U. S. A.* **2001,** *98* (18), 10037–41.

(6) Tsai, A. L.; Kulmacz, R. J., Prostaglandin H synthase: resolved and unresolved mechanistic issues. *Arch. Biochem. Biophys.* **2010,** *493* (1), 103–24.

(7) Dietz, R.; Nastainczyk, W.; Ruf, H. H., Higher oxidation states of prostaglandin H synthase. Rapid electronic spectroscopy detected two spectral intermediates during the peroxidase reaction with prostaglandin G2. *Eur. J. Biochem.* **1988,** *171* (1–2), 321–8.